american physiological society

JOURNAL OF APPLIED PHYSIOLOGY

J Appl Physiol 139: 341–354, 2025.
First published June 30, 2025; doi:10.1152/japplphysiol.00250.2025

RESEARCH ARTICLE

Cerebrovascular Control in Health and Disease: From Modeling to Translational Research

Cerebrovascular variability interactions after acute ischemic stroke: insights from directionality analysis based on transfer entropy

Francesca Gelpi,[1,2]* Beatrice Cairo,[2]* Vlasta Bari,[1,2] Beatrice De Maria,[3] Angela S. M. Salinet,[4] Man Y. Lam,[5] Osian Llwyd,[6] Jonathan Ince,[5] Jatinder S. Minhas,[5,7] Ronney B. Panerai,[5,7] and Alberto Porta[1,2]

[1]*Department of Cardiothoracic, Vascular Anesthesia and Intensive Care, IRCCS Policlinico San Donato, Milan, Italy;* [2]*Department of Biomedical Sciences for Health, University of Milan, Milan, Italy;* [3]*IRCCS Istituti Clinici Scientifici Maugeri, Milan, Italy;* [4]*Neurology Department, Hospital das Clinicas, School of Medicine, University of São Paulo, São Paulo, Brazil;* [5]*Cerebral Haemodynamics in Ageing and Stroke Medicine (CHiASM), Department of Cardiovascular Sciences, University of Leicester, Leicester, United Kingdom;* [6]*Wolfson Centre for Prevention of Stroke and Dementia, Department of Clinical Neuroscience, University of Oxford, Oxford, United Kingdom; and* [7]*NIHR Leicester Biomedical Research Centre, BHF Cardiovascular Research Centre, Glenfield Hospital, Leicester, United Kingdom*

Abstract

Dynamic cerebral autoregulation (CA) limits fluctuations of mean cerebral blood flow, approximated as mean cerebral blood velocity (MCBv) measured via transcranial Doppler ultrasound, in the presence of variations of mean arterial pressure (MAP). This mechanism is impaired after acute ischemic stroke (AIS). CA impairment is usually assessed by hypothesizing that MAP variations are completely responsible for MCBv changes, although disregarding the MCBv contributions to MAP variability. We exploited transfer entropy (TE) and conditional TE (CTE) to assess the strength of the directional interactions from MAP to MCBv and vice versa accounting for partial pressure of end-tidal carbon dioxide. Traditional markers were computed for comparison. We analyzed recordings from 34 control individuals (CTRL, age: 66 ± 7 yr) and 48 patients with AIS (age: 66 ± 13 yr) acquired within 48 h of stroke symptom onset. MCBv was recorded in both hemispheres including affected and unaffected hemispheres in patients with AIS. Patients with AIS exhibited hypertension and hypocapnia. After AIS MCBv diminished, especially in the affected hemisphere. TE and CTE decreased along the pressure-to-flow pathway as well. Both directional markers tend to increase along the flow-to-pressure arm irrespective of the hemisphere. Traditional indexes could not detect any difference. Our analysis suggests that the CA impairment was characterized by an imbalance of information transfer within the MCBv-MAP closed loop with a reduced importance of the pressure-to-flow and increased relevance of the flow-to-pressure arm. The study stresses the relevance of assessing MCBv-MAP relationship in closed loop, especially when variability of MAP and MCBv are considered.

NEW & NOTEWORTHY The study emphasizes the importance of understanding the closed-loop relationship between mean arterial pressure and mean cerebral blood velocity when characterizing cerebrovascular control. Directional analysis is particularly insightful in acute ischemic stroke because modifications occurring along the flow-to-pressure link complement the ones derived from the more traditionally examined pressure-to-flow pathway.

blood pressure variability; causality; cerebral autoregulation; cerebral blood flow; cerebrovascular control

INTRODUCTION

The dynamic component of cerebral autoregulation (CA) limits the variability of mean cerebral blood flow (MCBF) despite changes of mean arterial pressure (MAP) via suitable modifications of cerebrovascular resistances over a range of time scales spanning from a few seconds to minutes (1–3). Outside the MAP interval covered by the CA regime, ischemia accompanying insufficient oxygen supply to the brain or hyperemia associated with edema might occur because changes of MCBF follow proportionally those of MAP. Impairment of CA leads to a reduction of the MAP interval where CA is effective, thus increasing the likelihood that the brain could be exposed to periods of

*F. Gelpi and B. Cairo contributed equally to the work.
Correspondence: A. Porta (alberto.porta@unimi.it).
Submitted 31 March 2025 / Revised 30 April 2025 / Accepted 25 June 2025

hypo- or hyper-perfusion (4). Deterioration of CA worsens the outcome after major cerebrovascular events (5, 6) and might contribute to postural syncope and neurocognitive dysfunction (7, 8).

Globally, stroke is the second leading cause of death (9), and the projection for 2,030 indicates that its incidence rate will increase (9). In 85% of cases, stroke happens when the blood supply to the brain is stopped by a blood clot leading to ischemic stroke (10). Most strokes are ischemic (9) and associated in the acute phase with an impairment of CA (11–16). This impairment was observed more commonly in the affected hemisphere early after major ischemic stroke (12, 15, 16), although the deficit of CA was observed bilaterally when small vessels were involved (12, 15).

Probing the CA implies the use of an intervention inducing a relevant modification of MAP to evoke adjustments of MCBF (17, 18). Alternatively, spontaneous fluctuations of MAP and mean cerebral blood velocity (MCBv), taken as a surrogate of MCBF, as derived from a transcranial Doppler (TCD) device (19), can be exploited (20–29). Given that spontaneous variations of MAP are not induced as a consequence of an external stimulus, and their vascular origin cannot be taken for granted, MAP oscillations might be the effect of MCBv variations (26–29). Indeed, the closed-loop nature of the relationship between MCBv and MAP is well-known (26–29). In addition to the commonly assessed pressure-to-flow link (30), a flow-to-pressure pathway was revealed by the rise of MAP evoked by the elevation of the intracranial pressure, usually referred to as the Cushing reflex (31). Although the Cushing reflex was proposed as a survival vasopressor response, currently Cushing-like reflexes are believed to be always active in the brain, thus contributing continuously to the short-term regulation of arterial pressure (AP) (32–35) even at time scales as fast as the respiratory one (28, 36, 37). The feedback pathway from MCBv to MAP is usually disregarded in interventional studies of CA, mainly due to the relevance of the MAP changes imposed on the subject. Conversely, the closed-loop nature of the MAP-MCBv dynamic interactions should be considered when exploiting the MAP and MCBv spontaneous variability because the small amplitude of the fluctuations does not ensure the irrelevance of the contribution of MCBv changes to MAP variations, thus biasing the assessment of CA (38).

The aim of this study is to characterize the closed-loop relationship between MAP and MCBv after acute ischemic stroke (AIS) via a directional approach assessing transfer entropy (TE) applied to spontaneous fluctuations of MAP and MCBv. TE analysis separates the pressure-to-flow pathway, usually evaluated to characterize CA, from the flow-to-pressure one more frequently disregarded. TE analysis features the possibility of accounting for the slow variations of partial pressure of carbon dioxide (P_{CO_2}), that might mix up causal relationships between MAP and MCBv on both the time directions by driving a portion of their variability, via conditional TE (CTE). Recordings were carried out on both the right and left hemisphere of healthy control (CTRL) subjects and in patients with AIS on the affected (AFF) and unaffected (UNAFF) hemispheres.

MATERIALS AND METHODS

Ethics Statement

Data within the Leicester Cerebral Haemodynamics database were all collected through studies, which were performed in accordance with the Declaration of Helsinki for medical research involving humans. All contributing studies received ethical approval. More specifically, studies collecting control participant data received ethical approval from either the University of Leicester Ethics Committee (Reference No. jm591-c033) or the Northampton Research Ethics Committee (reference: 11/EM/0369). Studies contributing AIS data to the database received ethical approval from respective Research Ethics Committees, including: Leicestershire, Northamptonshire, and Rutland Research Ethics Committee (Reference No. 09/H0403/25); Nottingham Research Ethics Committee (Reference No. 11/EM/0016); North East – Newcastle & North Tyneside 1 Research Ethics Committee (Reference No. 14/NE/1003); East Midlands – Nottingham 1 Research Ethics Committee (Reference No. 15/EM/0485); and Wales Research Ethics Committee 1 (Reference No. 15/WA/0328).

Experimental Protocol

Data from 34 CTRL volunteers (age: 66 ± 7 yr, 17 male) and 48 patients with AIS (age: 66 ± 13 yr, 30 male) were extracted and retrospectively analyzed from the Leicester Cerebral Haemodynamics database. CTRL volunteers were defined as having no significant past medical history of cardiovascular, neurological, or respiratory disease (although well-controlled hypertension was allowed). Patients with AIS were recruited from an acute hospital within 48 h of symptom onset, with diagnosis confirmed by neuroimaging. Severity of AIS was typically mild-to-moderate, with a National Institutes of Health Stroke Scale (NIHSS) score value of 3.5 ± 2.4 at the time of recording. Oxford classification of stroke subtype included 2 total anterior circulation strokes, 19 partial anterior circulation strokes, 3 posterior circulation strokes, and 24 lacunar strokes. The average time from stroke symptom onset to TCD recording was 21.1 ± 12.4 h. Recorded comorbidities in patients suffering from AIS included hypertension, and in a small proportion, diabetes mellitus, ischemic heart disease, and degree of carotid atheroma. Exclusion criteria were poor insonation of at least one of the temporal bone windows and a history of atrial or ventricular arrhythmias. CTRL volunteers and patients with AIS were in conscious state. All the subjects gave written informed consent. Patients with AIS were enrolled at the Hyperacute Stroke Unit at University Hospitals of Leicester NHS Trust, Leicester, UK (13). CTRL subjects were recruited from hospital and university staff, and among patients' relatives. Investigations of the CTRL group were performed at the University of Leicester's Cerebral Haemodynamics in Ageing and Stroke Medicine (CHIASM) research laboratory, with minimal auditory or visual distraction, following the standard protocol for recordings at rest in supine position under spontaneous respiration (39). CTRL volunteers were asked to avoid heavy exercise, caffeine, alcohol, and nicotine for at least 12 h before attending the measurements. Subjects were instrumented to continuously monitor noninvasive AP using a cuff placed on the middle finger of the right hand via a volume-clamp device (Finapres Medical Systems, Enschede, The

Netherlands). The cerebral blood velocity (CBv) was measured from the middle cerebral artery using a TCD device (DopplerBoxX, Compumedics DWL, Singen, Germany). The measurements were performed bilaterally with 2-MHz probes supported by a headframe. In the AIS cohort, recordings were performed and analyzed for both the AFF and UNAFF hemispheres. In the CTRL group, recordings were performed bilaterally. Inhaled and exhaled P_{CO_2} was recorded using a capnogram (CAP) with a nasal cannula (Capnocheck Plus, Smiths Medical ASD Inc., St Paul, MN). Data were continuously acquired through a data acquisition system (PHYSIDAS, Department of Medical Physics, University Hospitals of Leicester, Leicester, UK) for subsequent offline analysis using a sampling rate of 500 Hz. A 5-min baseline recording was obtained with the head supported by one or two pillows.

Variability Series and Their Univariate Characterization

Signals were preprocessed as previously described (40). Briefly, any narrow spikes were identified on the CBv and AP and then removed by linear interpolation between the closest unaffected signal values. All signals were then low-pass filtered with an eight-order, zero-phase Butterworth filter with a cut-off frequency of 20 Hz. The MAP and MCBv were obtained as the integral under the curve computed between consecutive diastolic values divided by interdiastolic period. The resulting series were manually corrected in the case of missing beats or misdetections. The effect of ectopic beats or arrhythmic events was mitigated via linear interpolation between the closest values unaffected by arrhythmic beats. Corrections did not exceed 5% of the total sequence length. Periods of consecutive corrections were no longer than 4 s. All series were spline-interpolated in time domain, low-pass filtered with a fourth-order zero-phase Butterworth filter with a cutoff frequency of 0.5 Hz, and resampled at 1 Hz to obtain equally spaced samples in time. Sequences of 250 consecutive samples (i.e., 250 s) were selected with the onset randomly chosen within the recording.

The mean and variance of MAP and MCBv, namely μ_{MAP}, σ^2_{MAP}, μ_{MCBv}, and σ^2_{MCBv}, were computed and expressed in mmHg, $mmHg^2$, $cm \cdot s^{-1}$ and $cm^2 \cdot s^{-2}$, respectively. Power spectral density was calculated according to an autoregressive (AR) description of the series (41). The AR coefficients and variance of the noise feeding the AR model were estimated via the traditional least squares approach solved via Levinson–Durbin recursion (41). The optimal model order was optimized via the Akaike information criterion in the range from 4 to 16 (36, 42). The power of the MAP and MCBv series was computed as the variance of the spectral component whose central frequency fell in a specific frequency band (43). We chose the range of frequencies covering both the very low frequency and low frequency (LF) band (i.e., from 0.02 to 0.20 Hz) because it covered the time scales of the autonomic control (38). Indexes were expressed in absolute units, namely $mmHg^2$ and $cm^2 \cdot s^{-2}$, respectively, and were labeled LF_{MAP} and LF_{MCBv}. From the CAP signal, we computed the breath-by-breath series of partial pressure of end-tidal carbon dioxide ($P_{ET_{CO_2}}$). $P_{ET_{CO_2}}$, taken as a marker of partial pressure of alveolar carbon dioxide, was extracted as the sample of CAP at the end of the nearly horizontal line of CAP signal representing the expiration phase. Given that $P_{ET_{CO_2}}$ was extracted on a breath-by-breath basis, $P_{ET_{CO_2}}$ was aligned in the time domain and processed like MAP and MCBv, thus becoming fully synchronous with MAP and MCBv at 1 Hz. From the resampled $P_{ET_{CO_2}}$ series, we extracted the mean and variance, denoted with $\mu P_{ET_{CO_2}}$ and $\sigma^2 P_{ET_{CO_2}}$, and expressed in mmHg and $mmHg^2$, respectively. These markers were taken as descriptors of the partial pressure of arterial carbon dioxide and its variability, being in equilibrium with $P_{ET_{CO_2}}$. The respiratory frequency (f_R) was extracted from CAP signal as well and expressed in $breaths \cdot min^{-1}$. To prevent the potential confounding effect of respiration on the computed markers, we checked that the f_R did not fall in the LF band.

Characterization of CA via Bivariate Analysis

CA is usually characterized via tools jointly analyzing MAP and MCBv variability (38, 44). Frequency domain tools based on cross-spectral analysis were frequently used (21–24). The cross-spectral approach is based on a traditional model assessing the relationship from an input series to an output, while disregarding the possible presence of a feedback pathway (45). In the present study, a nonparametric approach based on fast Fourier transform (FFT) was exploited (38). The time domain MAP and MCBv variability series were upsampled from 1 Hz to 5 Hz and broken down into smaller overlapped sequences matching the constraints for the applications of FFT. The upsampling was carried out to adapt cross-spectral analysis to the standards provided in previous white papers (38, 44). The Welch's method was used to improve the consistency of the auto- and cross-spectral densities via averaging. The Hanning window was applied before each FFT to minimize spectral leakage. Superposition between frames was set to 50%. The transfer function (TF) was estimated as the ratio of the power cross-spectral density from MAP to MCBv variability ($C_{MCBv\ -\ MAP}$) to the power spectral density of MAP series. The TF gain (TFG) was computed as the modulus of the TF. TFG quantifies the amplitude of MCBv oscillation at the frequency f per unit amplitude of MAP oscillation at the same frequency. The TF phase (TFP) was computed as the phase of the TF. TFP indicates the lag at a specific frequency between MAP and MCBv, where positive phase shifts from 0 to $+\pi$ indicating that MCBv variations lead MAP changes, and negative values from 0 to $-\pi$ indicating that MCBv variations lag behind MAP changes. The squared coherence (K^2) was computed as the ratio of the squared modulus of $C_{MCBv\ -\ MAP}$ to the product of the power spectral densities of MAP and MCBv, where $K^2(f)$ ranges from 0 to 1, indicating, respectively, null and perfect linear association between MCBv and MAP series at each frequency f. TFG was expressed in $cm \cdot s^{-1} \cdot mmHg^{-1}$, TFP was expressed in radians (rad), and K^2 was dimensionless. The values of TFG, TFP, and K^2 were averaged within the LF band, namely from 0.07 to 0.20 Hz, being the range of frequencies where K^2 was more likely to be significant (38, 44).

The autoregulatory index (ARI) was assessed by comparing the step response derived from TF (46) to the theoretical step responses of the derivative filter describing the pressure-flow relationship in (17). Ten combinations of the filter's parameters correspond to 10 responses, and they were associated with different values of ARI ranging from absent CA (ARI = 0), namely MCBv follows completely MAP changes, to excellent CA (ARI = 9), namely variations of MCBv, resulting

from changes MAP, decay very rapidly over time leading to producing no consequence on MCBv after a few time constants. An ARI > 4 was considered a marker of efficient CA (17). The impulse response function was estimated via the inverse FFT applied to the TF from MAP and MCBv and integrated to obtain a numerical estimate of the unit step response. The theoretical unit step responses were derived from the Tiecks' model by feeding it with unit sustained step. Theoretical and predicted step responses were rescaled by dividing each sample by their own maximum absolute value (47). The theoretical curve derived from the Tiecks' model was compared with that derived from the TF-based analysis via normalized mean square error and the ARI value corresponding to the comparison with minimum figure was selected (46). The percentage of subjects with an effective CA (i.e., ARI > 4) was calculated for each group as well.

Estimation of TE and CTE

The method assesses the information transfer from the driver to the responder as the amount of information carried by the current value of the target series y that can be genuinely attributed to the source series x. In the TE approach, the information carried by the present sample of y due to the action of x was computed by separating it from the portion that can be derived from the past of y, while in the CTE calculation it was separated from the portion that can be attributed to the past of the conditioning series z as well. Before computing TE and CTE, all the variability series, namely x, y, and z, were normalized by subtracting the mean and by dividing the result by the standard deviation. We exploited a linear, parametric, model-based approach grounded on vector autoregressive class (48, 49) computing TE and CTE according to the Granger causality approach (50). The complete description of the models in the full and restricted universes of knowledge is given in APPENDIX along with the formulas used to compute TE and CTE. The identification of the coefficients of the models was carried out by solving the linear least squares problem via the Cholesky decomposition method (51). Each regression features the same number of coefficients that was optimized via the Akaike criterion for multivariate processes (49) in the range from 6 to 14. The number of coefficients was optimized in the full universe of knowledge, and it was maintained in the restricted one (49). A double regression approach was exploited because the identification procedure performed in the full universe of knowledge was repeated in the restricted universe of knowledge, thus leading to a different set of coefficients for the same portion of the model (49). The modeling approach requires the setting of the latency τ of the actions of the driver and confounding factor on the target signal, namely τ from x to y ($\tau_{x\to y}$) and τ from z to y ($\tau_{z\to y}$). The impact of the latency setting was monitored by testing the ability of TE in differentiating CTRL from AFF and from UNAFF data on both the pressure-to-flow and flow-to-pressure pathways. After selecting the latency describing the action of x on y and vice versa, the impact of latency of the action of the confounding factor z on the closed-loop interaction between x and y was monitored by checking the ability of CTE in differentiating CTRL from AFF and from UNAFF data as well. Latencies were varied from 0 to 5 s, where 0 s and 5 s indicate a possible impact by 1 s and 6 s, respectively. Longer latencies were not considered because TE and CTE decreased monotonically as a function of the time horizon used in resolving the uncertainty of y based on the behavior of x due to the presence of noise and additional factors unaccounted in the full universe of knowledge (52, 53). The simultaneous presence of latencies equal to 0 s was not tested because this situation referred to the unrealistic condition of closed-loop interactions without delays (43).

Testing the Null Hypothesis of MCBv-MAP Uncoupling

Since TE and CTE might be different from zero even in presence of full uncoupling, the significant difference of TE and CTE from zero was tested using the method of surrogates (54). Surrogates are artificial series built from the original ones according to some null hypothesis. Here the null hypothesis is the absence of dynamic interactions between MAP and MCBv, while all the univariate dynamic properties of the series, namely distribution of the values, linear autocorrelation, and nonlinear relationship between successive samples are preserved as much as possible. Uncoupled pairs in the case of TE analysis, or uncoupled triplets, in the case of CTE analysis, were generated via time-shifting method (55). The method shifted in time the presumed cause and confounding series, if present, with different latencies drawn randomly in the interval 45–80 s, although the effect series was left unaltered. Circular wrapping was exploited to preserve the original length of the series. One uncoupled pair, or one uncoupled triplet, was generated from each original pair, or triplet, recorded in any subject and hemisphere. When computing TE, or CTE, the same parameter setting was used over original and surrogate series. If TE, or CTE, computed over the original series was significantly above that derived from the surrogates with a $P < 0.05$, the null hypothesis of uncoupling was rejected, thus supporting that a significant information transfer was present in the original series.

Statistical Analysis

The Shapiro–Wilk normality test was used to test normality of the distributions. All indexes were computed on recordings of both left and right hemispheres in the CTRL cohort and compared between the two hemispheres via the paired t test, or the Wilcoxon signed-rank test when appropriate. Differences between information domain markers derived from original and surrogate data were checked via the same tests. An unpaired t test, or a Mann–Whitney rank sum test when appropriate, was applied to check the difference between CTRL and AIS groups over time-domain markers. After pooling together groups and hemispheres the same test was used to compare TE and CTE markers. One-way repeated measures analysis of variance (Dunnett's test for multiple comparisons), or Friedman repeated measures analysis of variance on ranks if appropriate (Dunnett's test for multiple comparisons), was used to compare the cerebrovascular control markers across hemispheres in the CTRL and AIS groups. Two-way analysis of variance (Holm–Sidak test for multiple comparisons) was used to compare TE and CTE indexes within the same group and differences across groups using the same information transfer index. Statistical

analysis was carried out using a commercial statistical program (Sigmaplot, v. 14.0, Systat Software, Inc., Chicago, IL). The level of significance of all the tests was set to 0.05.

RESULTS

Univariate Markers

Representative examples of variability series taken from a CTRL and AIS subject are shown in Fig. 1. In this representative comparison, an increase of μ_{MAP} and σ^2_{MAP} was observed in the patient with AIS (Fig. 1, *A* and *B*). The left and right MCBv series exhibits similar dynamics in the CTRL subject (Fig. 1, *C* and *E*). μ_{MCBv}, decreased in the AFF hemisphere (Fig. 1*D*) compared with the UNAFF one (Fig. 1*F*) and with the right and left hemisphere of the CTRL subject (Fig. 1, *C* and *E*). A tendency toward an increased σ^2_{MCBv} in the UNAFF hemisphere (Fig. 1*F*) compared with the AFF one (Fig. 1*D*) was visible. μPET_{CO_2} declined in the patient with AIS with a tendency toward a higher $\sigma^2 PET_{CO_2}$ (Fig. 1*H*) compared with the CTRL individual (Fig. 1*G*).

None of the computed indexes showed any statistically significant difference between the two hemispheres in the CRTL group. Therefore, all the analyses in the following were carried out using only the MCBv series obtained from one hemisphere selected at random in each CTRL subject.

Table 1 shows the univariate markers derived from variability series of MAP, CAP signal, and variability of PET_{CO_2} in CTRL and AIS populations. The AIS group featured higher μ_{MAP}, augmented σ^2_{MAP}, lower μPET_{CO_2}, and increased $\sigma^2 PET_{CO_2}$ compared with the CTRL one. LF_{MAP} and f_R did not vary across the two groups.

Table 2 summarizes the cerebrovascular parameters in the CTRL group and AIS population when distinguishing between AFF and UNAFF hemispheres. In the AFF hemisphere, we observed a lower μ_{MCBv} compared with CTRL subjects. No difference was observed when comparing μ_{MCBv} in the CTRL group and the UNAFF hemisphere of the AIS group. σ^2_{MCBv} and LF_{MCBv} did not vary across populations and hemispheres.

Testing the Null Hypothesis of MAP-MCBv Uncoupling

Table 3 lists the values of TE and CTE markers computed over the original and surrogate pairs. Analysis was carried out in the direction from MAP to MCBv and vice versa. Values present in Table 3 were computed with the latencies optimized to ensure the identification of the impact of AIS on the directionality from MAP to MCBv. Regardless of the group of measures, namely CTRL and type of hemisphere in the AIS individuals, TE markers computed over the original pairs were significantly higher than those calculated over surrogate uncoupled pairs. Remarkably, significant information transfer was observed in both directions. The same result was achieved when CTE indexes were calculated.

CA Indexes

Table 4 reports the CA indexes derived from power cross-spectral and ARI analyses. Regardless of the type of CA marker no differences were detected between CTRL subjects

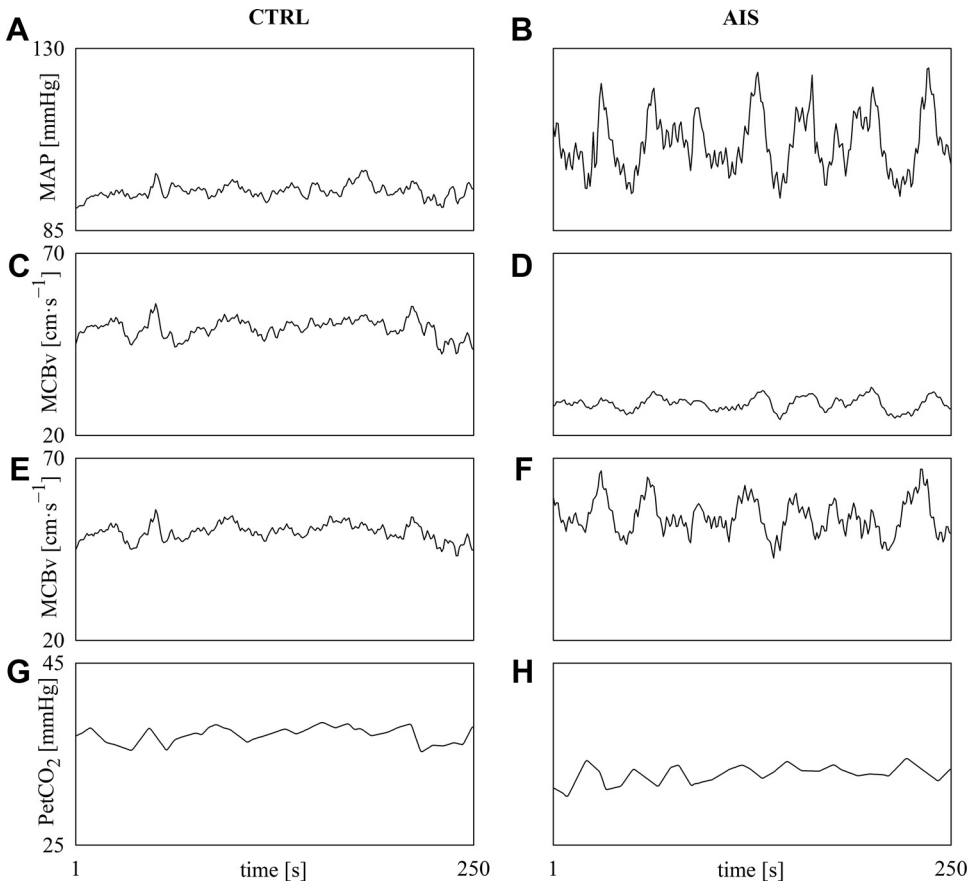

Figure 1. The line graphs show the variability series of MAP (*A*), MCBv recorded from the left (*C*) and right (*E*) hemisphere, and PET_{CO_2} (*G*) in a CRTL subject and those of MAP (*B*), MCBv recorded from the AFF (*D*) and UNAFF (*F*) hemisphere, and PET_{CO_2} (*H*) in a patient with AIS as a function of time expressed in seconds. AIS, acute ischemic stroke; MAP, mean arterial pressure; MCBv, mean cerebral blood velocity; PET_{CO_2}, end-tidal pressure of carbon dioxide.

Table 1. *MAP, CAP, and $P_{ET_{CO_2}}$ markers in CTRL and AIS groups*

Markers	CTRL	AIS
μ_{MAP}, mmHg	90.2 ± 8.4	103.1 ± 17.7*
σ^2_{MAP}, $mmHg^2$	6.0 ± 4.2	19.4 ± 17.3*
LF_{MAP}, $mmHg^2$	0.7 ± 0.8	2.8 ± 5.3
f_R, breaths·min^{-1}	17.6 ± 4.2	16.6 ± 5.2
$\mu P_{ET_{CO_2}}$, mmHg	38.3 ± 2.3	33.7 ± 3.9*
$\sigma^2 P_{ET_{CO_2}}$, $mmHg^2$	2.4 ± 9.3	4.9 ± 12.3*

Results are reported as means ± SD. AIS, acute ischemic stroke; CAP, capnogram; f_R, respiratory frequency from CAP signal; LF, low frequency; LF_{MAP}, LF power of the MAP series; MAP, mean arterial pressure; μ_{MAP}, MAP mean; $\mu P_{ET_{CO_2}}$, $P_{ET_{CO_2}}$ mean; σ^2_{MAP}, MAP variance; $\sigma^2 P_{ET_{CO_2}}$, $P_{ET_{CO_2}}$ variance; $P_{ET_{CO_2}}$, partial pressure of end-tidal carbon dioxide. *$P < 0.05$ vs. CTRL.

and AIS population after considering AFF and UNAFF hemispheres. The TFP_{LF} was always positive in all the groups. K^2_{LF} values were mostly above the physiological meaningful level of 0.30. In most of the subjects, ARI indicated an effective CA.

The grouped bar graphs of Fig. 2 show the type I error probability P computed when comparing TE calculated in CTRL subjects and patients with AIS when considering AFF (black bars) and UNAFF (white bars) hemisphere as a function of the latency of the MCBv-MAP dynamic interactions. Results relevant to $TE_{MAP\rightarrow MCBv}$ are shown in Fig. 2*A* as a function of $\tau_{MAP\rightarrow MCBv}$, whereas those relevant to the reverse pathway (i.e., $TE_{MCBv\rightarrow MAP}$) are depicted in Fig. 2*B* as a function of $\tau_{MCBv\rightarrow MAP}$. The level of significance below which comparison between groups was deemed to be significant (i.e., 0.05) was indicated as a dashed horizontal line in both panels. The type I error probability was below the level of significance for $\tau_{MAP\rightarrow MCBv} = 2$ s when comparing $TE_{MAP\rightarrow MCBv}$ computed over CTRL and AFF data and close to the significance at the same lag when comparing CTRL and UNAFF data (Fig. 2*A*). Over the reverse causal direction (i.e., from MCBv to MAP) the lowest values of type I error probability were detected at $\tau_{MCBv\rightarrow MAP} = 0$ s (Fig. 2*B*). Given the discriminative values of $\tau_{MAP\rightarrow MCBv} = 2$ s and $\tau_{MCBv\rightarrow MAP} = 0$ s, we selected this setting for all remaining analyses.

The error bar graphs of Fig. 3 show $TE_{MAP\rightarrow MCBv}$ (Fig. 3*A*) and $TE_{MCBv\rightarrow MAP}$ (Fig. 3*B*) as a function of the group (i.e., CTRL and AIS distinguishing AFF and UNAFF hemispheres). $TE_{MAP\rightarrow MCBv}$ decreased significantly in AFF data compared with CTRL, whereas $TE_{MAP\rightarrow MCBv}$ computed over UNAFF data was similar to the one calculated in CTRL group. $TE_{MCBv\rightarrow MAP}$ did not vary with AIS regardless of the type of hemisphere considered.

Table 2. *Cerebrovascular parameters in CTRL subjects and patients with AIS distinguishing AFF and UNAFF hemisphere*

Markers	CTRL	AFF	UNAFF
μ_{MCBv}, cm·s^{-1}	52.3 ± 13.0	41.7 ± 15.9*	45.5 ± 14.7
σ^2_{MCBv}, $cm^2 \cdot s^{-2}$	7.2 ± 6.3	6.4 ± 5.6	9.7 ± 9.9
LF_{MCBv}, $cm^2 \cdot s^{-2}$	0.7 ± 0.7	1.0 ± 1.8	0.9 ± 1.2

Results are reported as means ± SD. AIS, acute ischemic stroke; LF, low frequency; LF_{MCBv}, LF power of the MCBv series; MCBv, mean cerebral blood velocity; μ_{MCBv}, MCBv mean; σ^2_{MCBv}, MCBv variance. *$P < 0.05$ vs. CTRL.

Table 3. *TE and CTE computed over original and surrogate uncoupled pairs in CTRL subjects and patients with AIS distinguishing AFF and UNAFF hemisphere*

Group	Marker	Original Pairs	Surrogate Pairs
CTRL	$TE_{MAP\rightarrow MCBv}$	0.11 ± 0.05	0.02 ± 0.01*
	$CTE_{MAP\rightarrow MCBv}$	0.12 ± 0.05	0.01 ± 0.01*
	$TE_{MCBv\rightarrow MAP}$	0.34 ± 0.16	0.03 ± 0.01*
	$CTE_{MCBv\rightarrow MAP}$	0.34 ± 0.16	0.03 ± 0.01*
AFF	$TE_{MAP\rightarrow MCBv}$	0.09 ± 0.05	0.02 ± 0.01*
	$CTE_{MAP\rightarrow MCBv}$	0.08 ± 0.05	0.02 ± 0.01*
	$TE_{MCBv\rightarrow MAP}$	0.48 ± 0.37	0.03 ± 0.01*
	$CTE_{MCBv\rightarrow MAP}$	0.47 ± 0.38	0.02 ± 0.01*
UNAFF	$TE_{MAP\rightarrow MCBv}$	0.08 ± 0.05	0.02 ± 0.01*
	$CTE_{MAP\rightarrow MCBv}$	0.08 ± 0.02	0.02 ± 0.01*
	$TE_{MCBv\rightarrow MAP}$	0.52 ± 0.37	0.02 ± 0.01*
	$CTE_{MCBv\rightarrow MAP}$	0.52 ± 0.37	0.02 ± 0.01*

Results are reported as means ± SD. AFF, affected; AIS, acute ischemic stroke; CTE, conditional TE; MAP, mean arterial pressure; MCBv, mean cerebral blood velocity; TE, transfer entropy; UNAFF, unaffected. *$P < 0.05$ vs. original pairs.

The grouped bar graphs of Fig. 4 have the same structure as Fig. 2, but it shows the type I error probability P computed when comparing CTE calculated in CTRL subjects with AFF (black bars) and UNAFF (white bars) hemisphere of patients with AIS as a function of the latency of interactions from $P_{ET_{CO_2}}$ to MCBv (Fig. 4*A*) and from $P_{ET_{CO_2}}$ to MAP (Fig. 4*B*). The level of significance below which the comparison between groups was deemed to be significant (i.e., 0.05) was indicated as a dashed horizontal line in both panels. The type I error probability was below the level of significance regardless of the value of $\tau P_{ET_{CO_2}\rightarrow MCBv}$ and hemisphere (Fig. 4*A*). The type I error probability did not change with $\tau P_{ET_{CO_2}\rightarrow MAP}$ in Fig. 4*B*, being close to the level of significance only in the case of the comparison between CTRL and AFF data (Fig. 4*B*).

The error bar graphs of Fig. 5 show TE and CTE over the directions from MAP to MCBv (Fig. 5*A*) and from MCBv to MAP (Fig. 5*B*). Data were pooled together regardless of the group and hemisphere. Indexes were computed with $\tau_{MAP\rightarrow MCBv} = 2$ s, $\tau_{MCBv\rightarrow MAP} = 0$ s, $\tau P_{ET_{CO_2}\rightarrow MCBv} = 0$ s, and $\tau P_{ET_{CO_2}\rightarrow MAP} = 0$ s. No significant differences were detected between TE and CTE, and this result held regardless of the direction of interactions.

The grouped error bar graphs of Fig. 6 show TE (black bars) and CTE (white bars) over the direction from MAP to MCBv (Fig. 6*A*) and from MCBv to MAP (Fig. 6*B*) as a function of the group, namely CTRL and AIS when distinguishing the AFF and UNAFF hemisphere. Indexes were computed

Table 4. *Traditional CA indexes in CTRL subjects and patients with AIS from AFF and UNAFF hemisphere*

Markers	CTRL	AFF	UNAFF
TFG_{LF}, cm·s^{-1}·$mmHg^{-1}$	1.4 ± 0.5	1.4 ± 0.8	1.3 ± 0.8
TFP_{LF}, rad	0.6 ± 0.2	0.6 ± 0.4	0.6 ± 0.4
K^2_{LF}	0.8 ± 0.1	0.8 ± 0.2	0.8 ± 0.2
ARI	4.9 ± 1.5	4.7 ± 1.9	4.8 ± 2.2
ARI > 4, %	72	69	68

Results are reported as means ± SD and as percentage of subjects with ARI > 4. AIS, acute ischemic stroke; AFF, affected; ARI, autoregulatory index; K^2, squared coherence; K^2_{LF}, K^2 in the LF band; LF, low frequency; TFG, transfer function gain; TFP, transfer function phase; TFG_{LF}, TFG in the LF band; TFP_{LF}, TFP in the LF band; UNAFF, unaffected.

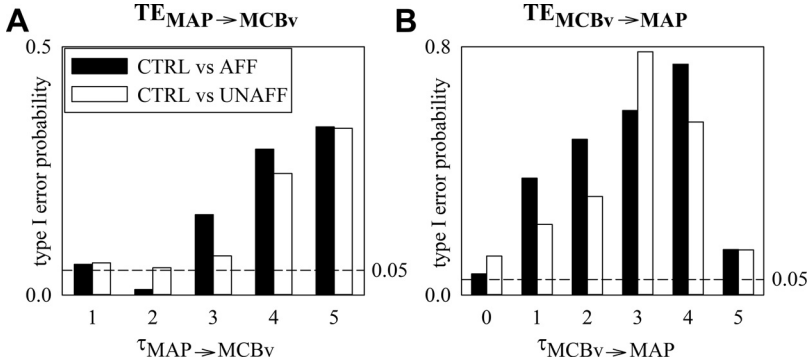

Figure 2. The grouped bar graphs show the type I error probability P when testing the difference of $TE_{x\to y}$ between CTRL and AFF groups (black bars) and between CTRL and UNAFF groups (white bars) as a function of the latency from x to y ($\tau_{x\to y}$). In (*A*), $TE_{x\to y}$ is computed with x = MAP and y = MCBv, whereas in (*B*), $TE_{x\to y}$ is calculated with x = MCBv and y = MAP. The dashed line indicates the level of significance of 0.05. AFF, affected; MAP, mean arterial pressure; MCBv, mean cerebral blood velocity; TE, transfer entropy; UNAFF, unaffected.

with $\tau_{MAP\to MCBv} = 2$ s, $\tau_{MCBv\to MAP} = 0$ s, $\tau PET_{CO_2\to MCBv} = 0$ s, and $\tau PET_{CO_2\to MAP} = 0$ s. No significant differences were detected between TE and CTE, and this result held regardless of the direction of interactions. Both $TE_{MAP\to MCBv}$ and $CTE_{MAP\to MCBv}$ decreased significantly in the AFF data compared with the CTRL group, although no significant differences were detected between CTRL and UNAFF data. The impact of AIS on $TE_{MCBv\to MAP}$ and $CTE_{MCBv\to MAP}$ was not evident due to the increased dispersion of markers reducing the statistical power of the comparison between CTRL and AIS groups. This conclusion held regardless of the type of hemisphere in patients with AIS.

DISCUSSION

The results of this study can be summarized as follows: *1*) latency setting in TE and CTE analyses allowed the identification of the impact of AIS on the directionality from MAP to MCBv; *2*) CTRL subjects and patients with AIS exhibited significant closed-loop dynamic interactions between MAP and MCBv at the selected values of latency; *3*) AIS induced hypertension in association with a reduced μ_{MCBv}, more evident in the AFF; *4*) AIS affected directionality of MAP-MCBv dynamic interactions, especially in the AFF hemisphere; *5*) TE was able to detect CA impairment in the AFF hemisphere of patients with AIS, although CA was preserved in the UNAFF one; *6*) computation of CTE obtained by conditioning out PET_{CO_2} did not modify conclusions in AIS group compared with those derived from unconditional TE.

Latency Setting Ensures the Identification of the Impact of AIS on the Directionality from MAP to MCBv

In previous studies (27, 28, 36), the latencies used in modeling the closed-loop dynamic interactions between MAP and MCBv variability were decided according to physiological considerations and MAP-MCBv cross-correlation. This evaluation was based on an assessment of the lag where the first local, negative, minimum of cross-correlation was detected with MAP changes leading MCBv variations, and the first local, positive, maximum of cross-correlation was found with MCBv changes leading MAP variations (56, 57). The latency of the action of MAP on MCBv leading to minimal negative cross-correlation was longer than that from MCBv to MAP leading to maximal positive cross-correlation (56, 57). This result agrees with the rapidity of pressure-sensitive mechanoreceptors in the brain sensing changes of intracranial pressure and evoking MAP changes via Cushing-like reflex (35, 58) compared with the slower inertial and capacitive hemodynamic responses adjusting MCBv in response to variations of MAP, especially when resistive components are negligible (35, 59). Based on these considerations, the latencies from MCBv to MAP, namely $\tau_{MCBv\to MAP}$, and from MAP to MCBv, namely $\tau_{MAP\to MCBv}$, were set to 0 s and 2 s (i.e., within a time interval of 1 s and 3 s, respectively) (27, 28, 36). This setting ensures the greatest speed of the flow-to-pressure pathway compared with the pressure-to-flow one (35, 56–59), it is compatible with the latency between hypotension and subsequent decrease of cerebrovascular resistance observed after thigh cuff deflation and sit-to-stand maneuver (60), and it preserves the relative difference between the two latencies as the one detected according to cross-correlation analysis, namely 2 s (56, 57). In addition, the selected short latencies limit the impact of the well-known monotonic decrease of TE as a function of the time horizon of prediction in physiological series due to presence of noise and insufficient description of confounding factors (52, 53).

In the present study, we adopted a different strategy for the selection of $\tau_{MCBv\to MAP}$ and $\tau_{MAP\to MCBv}$ grounded on a group-level optimization. We monitored the ability of TE to separate CTRL from AFF and UNAFF data as a function of

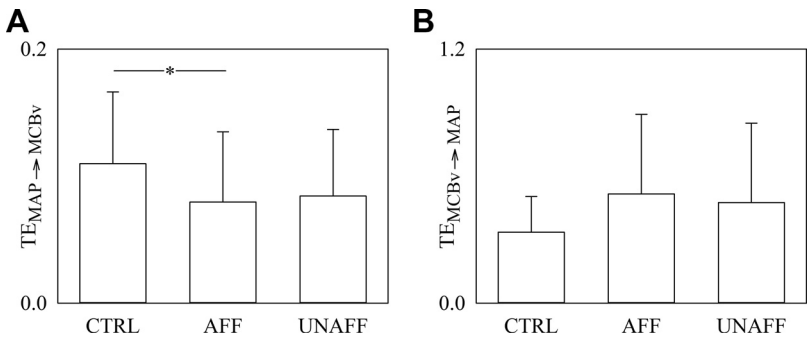

Figure 3. The error bar graphs show $TE_{MAP\to MCBv}$ (*A*) and $TE_{MCBv\to MAP}$ (*B*) as a function of the group (i.e., CTRL and AIS distinguishing between AFF and UNAFF hemisphere). TEs were computed with $\tau_{MAP\to MCBv} = 2$ s and $\tau_{MCBv\to MAP} = 0$ s. Data were represented as means + SD. AFF, affected; AIS, acute ischemic stroke; MAP, mean arterial pressure; MCBv, mean cerebral blood velocity; TE, transfer entropy; UNAFF, unaffected. *$P < 0.05$ vs. CTRL.

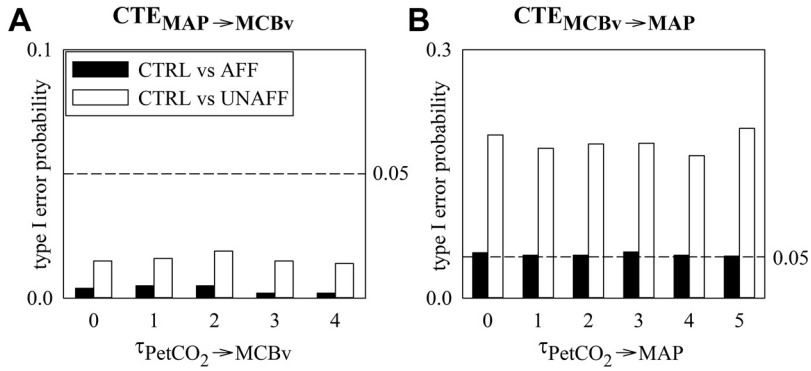

Figure 4. The grouped bar graphs show the type I error probability P when testing changes of $CTE_{x\to y}$ between CTRL and AFF groups (black bars) and between CTRL and UNAFF groups (white bars) as a function of the latency from z to y ($\tau_{z\to y}$). In (*A*), $CTE_{x\to y}$ is computed when x = MAP, y = MCBv, and the conditioning series is $P_{ET}CO_2$, whereas in (*B*), $CTE_{x\to y}$ is calculated when x = MCBv, y = MAP, and the conditioning series is $P_{ET}CO_2$. The dashed line indicates the level of significance of 0.05. The latency from MAP to MCBv was set to 2 s and that from MCBv to MAP to 0 s. AFF, affected; CTE, conditional TE; MAP, mean arterial pressure; MCBv, mean cerebral blood velocity; $P_{ET}CO_2$, end-tidal pressure of carbon dioxide; UNAFF, unaffected.

$\tau_{MCBv\to MAP}$ and $\tau_{MAP\to MCBv}$, and we selected the latency pair ($\tau_{MAP\to MCBv}$ and $\tau_{MCBv\to MAP}$) that allowed the strongest separation in the AIS population between the cerebrovascular control of AFF and UNAFF hemispheres using TE. Remarkably, the pair that allowed the detection of the minimum value of type I error probability when comparing CTRL with AFF and UNAFF data was $\tau_{MAP\to MCBv} = 2$ s and $\tau_{MCBv\to MAP} = 0$ s, thus supporting the idea that the latency setting adopted in our previous works could provide the best choice even when the purpose is the separation of different groups.

In previous works (28), the latencies of $P_{ET}CO_2$ on both arms of the MCBv-MAP closed loop, namely $\tau P_{ET}CO_{2\to MAP}$ and $\tau P_{ET}CO_{2\to MCBv}$, were set to 0 s (i.e., within a time interval of 1 s). This choice was supported by physiological considerations based on the rapidity of the mechanical effect of intrathoracic pressure on AP driven by modifications of venous return and stroke volume (61, 62) and the speed of the impact of movements of cerebrospinal fluid, driven again by changes of intrathoracic pressure, on intracranial pressure and MCBv (37). In the present work, we monitored the effect *of* $\tau P_{ET}CO_{2\to MCBv}$ and $\tau P_{ET}CO_{2\to MAP}$ on the separation between CTRL and AIS data, while maintaining the latency pair ($\tau_{MAP\to MCBv} = 2$ s and $\tau_{MCBv\to MAP} = 0$ s) adopted according to the TE analysis. Even the process of the optimization of $\tau P_{ET}CO_{2\to MCBv}$ and $\tau P_{ET}CO_{2\to MAP}$ was carried out at group level. Remarkably, conclusions derived from CTE did not depend on the selection of $\tau P_{ET}CO_{2\to MCBv}$ and $\tau P_{ET}CO_{2\to MAP}$, given that type I error probability was unvaried as a function of the latency from $P_{ET}CO_2$ to MCBv and from $P_{ET}CO_2$ to MAP. This conclusion held regardless of the hemisphere. This result supports the irrelevance of conditioning out $P_{ET}CO_2$ variability when modeling the closed-loop dynamic interactions between MAP and MCBv.

Significant Closed-Loop MCBv-MAP Dynamic Interactions are Observed in Both CTRL and AIS Groups

Standard approaches based on cross-spectral analysis assume open-loop interactions, usually from MAP to MCBv, while disregarding the feedback from MCBv to MAP (38, 45). In addition, even causality is poorly accounted for, given the ambiguities of phases when converted into delays or advancements due to Fourier phase circularity (45). Comparison with uncoupled surrogate pairs indicated that information transfer is significant on both causal directions of interactions, namely from MAP to MCBv and vice versa, in both CTRL and AIS groups and in the AIS group regardless of the hemisphere. This result supports the conclusion that mechanisms regulating dynamic interactions between MAP and MCBv are still present and working in patients with AIS. This result stresses the importance of accounting for both directions of interaction when CA is evaluated from spontaneous variability of MAP and MCBv likely because the smallness of the spontaneous variations of MAP might not allow one to disregard the eventual contribution to the MAP variability associated with the activation of the flow-to-pressure pathway. The need of considering the closed-loop relationship between MAP and MCBv when describing their spontaneous dynamic interactions was stressed in several studies (26–29, 36). This closed-loop condition results from the hemodynamic laws setting the relationship from MAP to MCBv (30, 59) and from the ability of brain receptors in sensing small changes of intracranial pressure as well as signals characterizing neural activity, hypoxic states, and ischemic environment and activating pressure responses (32–35, 63). Remarkably, our data suggest that this consideration held for both CTRL and AIS groups, even though the strength of interactions varied along the closed loop because the TE from MAP to MCBv decreased in

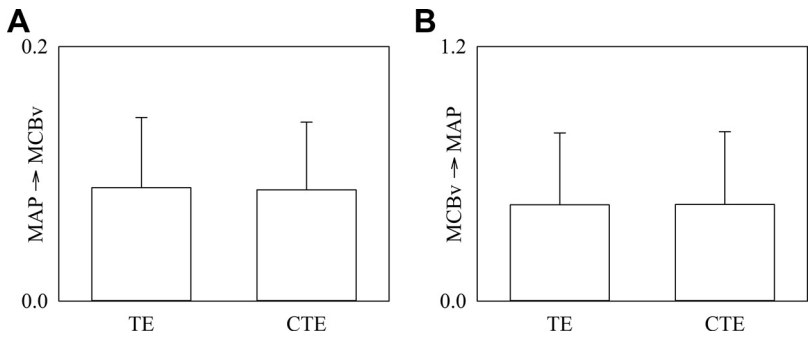

Figure 5. The error bar graphs compare TE and CTE in the direction from MAP to MCBv in (*A*) and in the reverse time, namely from MCBv to MAP, in (*B*). The data were pooled together regardless of the group and hemisphere. TE and CTE were computed with $\tau_{MAP\to MCBv} = 2$ s, $\tau_{MCBv\to MAP} = 0$ s, $\tau P_{ET}CO_{2\to MCBv} = 0$ s, and $\tau P_{ET}CO_{2\to MAP} = 0$ s. Data were represented as means + SD. CTE, conditional TE; MAP, mean arterial pressure; MCBv, mean cerebral blood velocity; TE, transfer entropy.

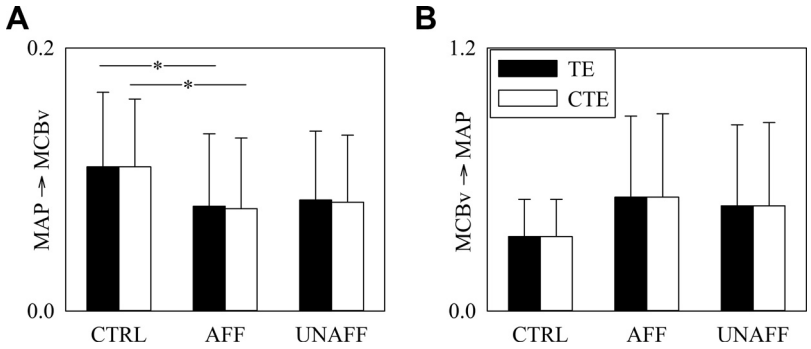

Figure 6. The grouped error bar graphs compare TE and CTE in the direction from MAP to MCBv in (*A*) and in the reverse time, namely from MCBv to MAP, in (*B*) as a function of the group, namely CRTL and AIS when distinguishing AFF and UNAFF hemisphere. TE and CTE were computed with $\tau_{MAP \rightarrow MCBv} = 2$ s, $\tau_{MCBv \rightarrow MAP} = 0$ s, $\tau PET_{CO_2 \rightarrow MCBv} = 0$ s, and $\tau PET_{CO_2 \rightarrow MAP} = 0$ s. Data were represented as means + SD. $^*P < 0.05$ vs. CTRL. AIS, acute ischemic stroke; CTE, conditional TE; MAP, mean arterial pressure; MCBv, mean cerebral blood velocity; TE, transfer entropy.

the AFF hemisphere, whereas TE in the reverse direction tended to increase.

Patients with AIS Feature a Reduced MCBv and Hypertension

The observed rise of μ_{MAP} is taken as a sign of the activation of the flow-to-pressure pathway that might be related to the increase of intracranial pressure associated with the development of cerebral edema and/or the physiological response to a hypoxic/ischemic brain state in the attempt to favor perfusion of the penumbral tissue (35, 64). Given the link of sympathetic tone and its variability to the amplitude of the AP variations (65), the increase of σ^2_{MAP} can be taken as indicative of the sympathetic activation accompanying AIS (66). The decrease of μ_{MCBv} despite the rise of μ_{MAP} suggests that the elevation of MAP is insufficient to preserve MCBv as a likely consequence of the elevation of intracranial pressure, the increase of cerebral resistances associated with sympathetic vasoconstriction and the derangement of hemodynamic properties of the vasculature in the infarcted areas and its surroundings (64, 66). The increase of μ_{MAP} in presence of a decrease of μ_{MCBv}, particularly evident in the AFF hemisphere, suggested the limited effect of the vasopressor reflex in coping with hypoperfusion in our AIS cohort.

AIS Affects Directionality of MCBv-MAP Dynamic Interactions

In patients with AIS, MAP was genuinely capable of driving modifications of MCBv, although MAP changes were also uniquely associated with MCBv fluctuations, thus indicating the closed-loop nature of the MCBv-MAP relationship in patients with AIS. These closed-loop interactions were observed in the CTRL group as well. In healthy individuals, the concomitant information exchange along the pressure-to-flow and flow-to-pressure pathways was observed even in the presence of experimental challenges increasing the amplitude of MAP fluctuations, such as during head-up tilt and active standing. This finding was taken as an indication of preserved CA (26–29, 36). Remarkably, in the present study, we reported an imbalance of the information exchange between MAP and MCBv variability in the AIS group. Indeed, patients with AIS featured the concomitant decrease of the TE along the pressure-to-flow arm of the closed loop, although the TE in the reverse direction remained unaltered, thus suggesting that the flow-to-pressure pathway is gaining importance compared with the pressure-to-flow arm. The increase of TE in the AIS group along the flow-to-pressure pathway was not significant due to the greater variability of TE compared with the same marker in the reverse pathway and this result, indicating a more variable individual response along the flow-to-pressure pathway in patients with AIS, requires further investigation. The increase of the information transfer from MCBv to MAP could be interpreted as the effect of the activation of Cushing-like reflexes that attempt to react to brain hypoperfusion by driving a MAP rise. However, the significant decrease of the TE from MAP to MCBv suggested that the Cushing-like reflexes were not successful in eliciting the expected modification of MCBv due to the overly weak performance of the pressure-to-flow link. The excessively reduced coupling in the direction from MAP to MCBv could be the consequence of a worsening of CA because it might suggest a limited coordination among all the mechanisms playing a role in shaping the response of CA to MAP changes, being related to damage to the cerebral vasculature, edema formation, and subsequent increases in intracranial pressure induced by AIS (64).

TE Detects the Early Impact of AIS on CA

Traditional assessment of CA based on cross-spectral analysis of MAP and MCBv variability series suggested that an increased TFG, a less positive or negative TFP, and an increased K^2 indicating a greater strength of MAP-MCBv association, or null values of K^2 suggesting full MAP-MCBv uncoupling, might be indicators of CA impairment (21–24). More recent approaches based on information transfer and spectral causality indicated that both an increased information transfer from MAP to MCBv (26) or dramatically limited genuine contribution of MAP to prediction of MCBv variations, especially visible in some frequency bands (27), allowed the separation of subjects with preserved and impaired CA. In the present study, TE was able to detect the CA impairment. It took the form of decreased information transfer from MAP to MCBv when CTRL subjects were compared with the data acquired from the AFF hemisphere of patients with AIS. Considering the hypocapnia of the AIS group, it could be hypothesized that the decrease of TE in AIS would be even more evident if CTRL and AIS groups were normalized to the same μPET_{CO_2} (67). However, this decrease did not lead to a situation in which the genuine contribution of MAP changes to the MCBv variability was fully abolished because the TE was above the level set by uncoupled surrogates. The decrement of TE from MAP to MCBv might be even indicative of a CA improvement, but it occurred with an unvaried information transfer in the reverse causal direction that suggests an activation of

Cushing-like reflexes in the attempt of restoring brain perfusion. We suggest that the combination of the worsened ability of MAP changes to genuinely drive MCBv variations and an unvaried strength of the coupling in the reverse pathway is the pattern that indicates the CA impairment in the AFF hemisphere. Remarkably, in the UNAFF hemisphere, a similar activation of the flow-to-pressure pathway was not accompanied by a significant decrease of the information transferred along the pressure-to-flow arm of the MCBv-MAP closed loop, thus indicating a sort of preservation of CA. However, the absence of differences between AFF and UNAFF hemispheres suggests that the variation of cerebrovascular control in AIS group is independent of the hemisphere, thus being a homogenous condition affecting the entire brain. This conclusion was confirmed when the variability of $P_{ET}CO_2$ was conditioned out. The greater impact of AIS on the AFF hemisphere in our population agrees with the notion present in literature suggesting that in AIS with moderate severity the impact is greater on the AFF hemisphere (12, 15, 16). Remarkably, traditional cross-spectral indexes and ARI were not able to detect any sign of CA impairment even though it was expected in moderate-to-severe AIS (11–16). This result might be the consequence of hypocapnia observed in our AIS cohort. Indeed, hypocapnia has a strong influence on CA and could explain the lack of differences compared with the CTRL group (67). It could be hypothesized that the differences in TF indexes and ARI could emerge if both groups had similar $\mu P_{ET}CO_2$. However, it cannot be excluded that the observed limited power of cross-spectral markers could be the consequence of the intrinsic weakness of these descriptors in coping with causality and closed-loop dynamic interactions (45, 54).

CTE Does Not Improve CA Characterization in AIS Group Compared with TE

It is well known that PCO_2 is a confounding factor of CA (35, 44), and it should be included in models describing the MCBv-MAP dynamic interactions. The confounding effect results from the fact that modifications of the MCBF might occur in response to the same amplitude of MAP changes in the presence of different PCO_2 levels, given that hypercapnia leads to cerebral vasodilation and increased MCBF, although hypocapnia causes vasoconstriction and decreased MCBF. TE and CTE were similar, and this result held regardless of the direction of the interactions and group. This finding suggests that $P_{ET}CO_2$ did not contribute significantly to the information transferred from MAP to MCBv and vice versa. This conclusion might appear to be surprising given the known impact of respiration on intracranial pressure (28, 36, 37) and the role played by the regulation of PCO_2 on cerebrovascular control (67, 68). However, it should be noted that fluctuations of $P_{ET}CO_2$ occur below the respiratory rate in the very low-frequency band, whereas short-term analysis allows a more reliable study of dynamic interactions at faster time scales. The present analysis suggests that the variability of $P_{ET}CO_2$ did not contribute to genuinely driving a significant portion of fluctuations of MCBv. This result stresses that accounting for $P_{ET}CO_2$ might be irrelevant when describing the dynamic component of CA from spontaneous changes of MAP and MCBv. This conclusion agrees with a previous assessment from our group in a completely different context (36). We suggest that conclusions might be different whether the analysis was focused on the very low frequency band by extending the length of the series above the usual 5-min recordings (29). Conversely, accounting for $\mu P_{ET}CO_2$ is very important when assessing the static component of CA due to the remarkable impact of the static level of $P_{ET}CO_2$ on the brain circulation (67).

Limitations of the Study and Future Developments

The main limitation of using TCD to estimate cerebral blood flow is that it measures CBv, which is considered equivalent to cerebral blood flow, only if the vessel diameter does not vary. Previous studies support the use of CBv because only minor changes of diameter (<4%) in response to AP variations or hypocapnia were observed (69). Autonomic control plays an important role in governing MCBv-MAP dynamic interactions (70) both on the pressure-to-flow link (71) and in the reverse pathway (29). Future studies could investigate the role played by the activation of sympathetic control during AIS in modulating the CA impairment. In our protocol, the $P_{ET}CO_2$ fluctuated within a very limited range. Testing whether stronger variations of PCO_2 could change the conclusions based on CTE is needed. Moreover, the mechanical impact of respiration on intracranial pressure was not considered, although it could be an important confounding factor for directionality analysis (28, 36, 37). The application of a specific respiratory pattern, such as slow breathing, could give even more insight into the information exchange within the MCBv-MAP closed loop and conditioning effects. Finally, we investigated the acute phase of AIS, focusing on the first 48 h after symptoms onset. Investigating the long-term effect of AIS at different times and via long follow-up could help understanding if the closed-loop MCBv-MAP dynamic interactions observed in this study could evolve overtime. Given that we considered AIS of mild-to-moderate severity, analysis could be extended to more severe AIS. The issue of the separate optimization of the latencies over the feedback and feedforward pathway in a closed-loop system requires the application of specific methods and ad hoc tests in the specific context of the characterization of MCBv-MAP dynamic interactions. Therefore, we preferred a heuristic, and simpler, approach based on the ability of our metric to differentiate groups to optimize latencies. This strategy might have increased the likelihood of finding significant between-group differences. We advocate the application of specific approaches of latency optimization in the same context to confirm the validity of our conclusions. Some recent advancements in the information domain led to the decomposition of information transfer into frequency components (72, 73). These approaches might deserve application because information-theoretic metrics can be computed in frequency bands where CA seems to be more active, thus focusing the analysis on specific temporal scales.

Conclusions

The study applied a closed-loop directional approach to characterize cerebrovascular control after AIS from the spontaneous variability of MAP and MCBv. The approach allowed one to condition out the breath-by-breath changes of $P_{ET}CO_2$ while assessing the strength of the directed interactions from MAP to MCBv and vice versa. The study emphasized

the importance of investigating the closed-loop relationship because the significant decrease of the coupling strength from MAP to MCBv, likely to be the result of the derangement of the hemodynamic properties of the vasculature and edema formation, was accompanied by an increase of the importance of the reverse arm, likely to be activated by the increase of intracranial pressure, brain hypoperfusion, and ischemia. Our analysis reduces the relevance of accounting $P_{ET_{CO_2}}$ fluctuations when studying the dynamic variability interactions between MAP and MCBv as a likely effect of the impact of $P_{ET_{CO_2}}$ variability in frequency bands that are not examined in this study. The directional analysis might be particularly helpful when exploiting MAP and MCBv variability, especially in populations where traditional markers of CA might fail in detecting the impairment of cerebrovascular control, such as in this particular AIS group. We recommend the application of this technique when assessing CA in AIS and when monitoring it overtime and during follow-up.

APPENDIX

Linear Model-Based Assessment of TE and CTE

We exploited a linear, parametric, model-based approach grounded on vector autoregressive class (48, 49) computing TE and CTE according to the Granger causality approach comparing the representation of the effect series y in a full universe of knowledge to that in the restricted universe of knowledge excluding the cause series x (50). The full and restricted universes of knowledge were suitably defined to eventually account for confounding factors. We defined *1*) the full universe of knowledge $\Omega = \{x, y, z\}$ accounting explicitly for the confounding series z mixing up the causal relationship from the cause x to the effect y; *2*) the full universe of knowledge $\Omega\backslash\{z\} = \{x, y\}$ disregarding the confounding factor z when describing the causal relationship from x to y; *3*) the restricted universe of knowledge $\Omega\backslash\{x\} = \{y, z\}$ obtained from Ω after excluding the presumed cause x while accounting for the confounding factor z; *4*) the restricted universe of knowledge $\Omega\backslash\{x, z\} = \{y\}$ obtained from Ω after excluding the presumed cause x while disregarding the confounding factor z.

TE was computed by comparing the description of y in the full universe of knowledge $\Omega\backslash\{z\}$ to that in the restricted universe of knowledge $\Omega\backslash\{x, z\}$, thus disregarding the impact of z on the causal relationship from x to y. The dynamics of y in $\Omega\backslash\{z\}$ is described as an AR model of y with an exogenous (X) part on x (ARX) as:

$$y_i = \sum_{k=1}^{p} a_{\Omega\,\{z\},k} \times y_{i-k} + \sum_{k=\tau_{x\to y}}^{p+\tau_{x\to y}-1} b_{\Omega\,\{z\},k} \times x_{i-k} + w_{y|\Omega\,\{z\},i}, \quad (A1)$$

whereas the dynamics of y in $\Omega\backslash\{x, z\}$ is modeled as an AR model of y as:

$$y_i = \sum_{k=1}^{p} a_{\Omega\,\{x,z\},k} \times y_{i-k} + w_{y|\Omega\,\{x,z\},i}, \quad (A2)$$

where $a_{\Omega\backslash\{z\},k}$ and $a_{\Omega\backslash\{x,z\},k}$ with $k = 1,\ldots, p$ is the coefficients of the autoregression on y; $b_{\Omega\backslash\{z\},k}$ are the coefficients of cross-regression on x with $k = \tau_{x\to y},\ldots, p + \tau_{x\to y}-1$; $w_{y|\Omega\backslash\{z\}}$ and $w_{y|\Omega\backslash\{x,z\}}$ are white Gaussian noise with 0 mean and variances $\lambda^2_{y|\Omega\,\{z\}}$ and $\lambda^2_{y|\Omega\,\{x,z\}}$, respectively; $\tau_{x\to y}$ is the latency from x to y; p is the model order; and i is the time index. Defined the prediction error as the difference between the current sample of y and its best prediction based on the considered models, the prediction error variances $\sigma^2_{y|\Omega\,\{x,z\}}$ and $\sigma^2_{y|\Omega\,\{x,z\}}$, being the estimates of $\lambda^2_{y|\Omega\,\{z\}}$ and $\lambda^2_{y|\Omega\,\{x,z\}}$, were computed in $\Omega\backslash\{z\}$ and $\Omega\backslash\{x, z\}$, respectively. The TE from x to y, labeled $TE_{x\to y}$, was computed as $0.5 \cdot \log(\sigma^2_{y|\Omega\,\{x,z\}}/\sigma^2_{y|\Omega\,\{z\}})$. $TE_{x\to y}$ represents the decrement of uncertainty when the presumed cause x is included in $\Omega\backslash\{x, z\}$, thus assessing the genuine contribution of x to the information carried by y when the confounding factor z was disregarded. $TE_{x\to y}$ is greater than 0, dimensionless, and directional (i.e., $TE_{x\to y}$ is different from $TE_{y\to x}$). Higher values of $TE_{x\to y}$ represent a greater strength of the coupling from x to y. $TE_{x\to y}$ was computed with x = MAP and y = MCBv, thus assessing $TE_{MAP\to MCBv}$ along the pressure-to-flow pathway with the latency $\tau_{MAP\to MCBv}$. After reversing the role of x and y, we calculated $TE_{MCBv\to MAP}$ along the flow-to-pressure link using the latency $\tau_{MCBv\to MAP}$.

CTE was calculated by comparing the description of y in the full universe of knowledge Ω to that in the restricted universe of knowledge $\Omega\backslash\{x\}$, thus accounting for the impact of z on the causal relationship from x to y. The dynamics of y in Ω is described as an AR model of y with a double exogenous (XX) part on x and z (ARXX) as:

$$y_i = \sum_{k=1}^{p} a_{\Omega,k} \times y_{i-k} + \sum_{k=\tau_{x\to y}}^{p+\tau_{x\to y}-1} b_{\Omega,k} \times x_{i-k} + \sum_{k=\tau_{z\to y}}^{p+\tau_{z\to y}-1} c_{\Omega,k} \times z_{i-k} + w_{y|\Omega,i}, \quad (A3)$$

whereas the dynamics of y in $\Omega\backslash\{x\}$ is modeled as an AR model of y with an exogenous (X) part on z (ARX) as:

$$y_i = \sum_{k=1}^{p} a_{\Omega\,\{x\},k} \times y_{i-k} + \sum_{k=\tau_{z\to y}}^{p+\tau_{z\to y}-1} c_{\Omega\,\{x\},k} \times z_{i-k} + w_{y|\Omega\,\{x\},i}, \quad (A4)$$

where $a_{\Omega,k}$ and $a_{\Omega\backslash\{x\},k}$ with $k = 1,\ldots, p$ is the coefficient of the autoregression on y; $b_{\Omega,k}$ is the coefficients of cross-regression on x with $k = \tau_{x\to y},\ldots, p + \tau_{x\to y}-1$; $c_{\Omega,k}$ and $c_{\Omega\backslash\{x\},k}$ are the coefficients of cross-regression on z with $k = \tau_{x\to z},\ldots, p + \tau_{x\to z}-1$; $w_{y|\Omega}$ and $w_{y|\Omega\backslash\{x\}}$ are white Gaussian noises with 0 mean and variances $\lambda^2_{y|\Omega}$ and $\lambda^2_{y|\Omega\,\{x\}}$, respectively; and $\tau_{x\to y}$ and $\tau_{z\to y}$ are the latencies from x to y and from z to y, respectively; and p is the model order. After computing the prediction error variances $\sigma^2_{y|\Omega}$ and $\sigma^2_{y|\Omega\,\{x\}}$ being the estimates of $\lambda^2_{y|\Omega}$ and $\lambda^2_{y|\Omega\,\{x\}}$ in Ω and $\Omega\backslash\{x\}$, respectively, the CTE from x to y given z, labeled $CTE_{x\to y}$, was evaluated as $0.5 \times \log(\sigma^2_{y|\Omega\,\{x\}}/\sigma^2_{y|\Omega})$. $CTE_{x\to y}$ represents the decrement of uncertainty when the presumed cause x is included in $\Omega\backslash\{x\}$, thus assessing the genuine contribution of x to the information carried by y when the confounding factor z was accounted for. $CTE_{x\to y}$ is greater than 0, dimensionless, and directional (i.e., $CTE_{x\to y}$ is different from $CTE_{y\to x}$). Higher values of $CTE_{x\to y}$ represent a greater strength of the coupling from x to y given z. $CTE_{x\to y}$ was computed with x = MAP, y = MCBv, and $z = P_{ET_{CO_2}}$, thus

assessing $CTE_{MAP\rightarrow MCBv}$ along the pressure-to-flow pathway conditioned on $P_{ET}CO_2$ using the latencies $\tau_{MAP\rightarrow MCBv}$ and $\tau P_{ET}CO_2\rightarrow MCBv$. After reversing the role of x and y, we calculated $CTE_{MCBv\rightarrow MAP}$ along the flow-to-pressure link conditioned on $P_{ET}CO_2$ using the latencies $\tau_{MCBv\rightarrow MAP}$ and $\tau_{MCBv\rightarrow}P_{ET}CO_2$. Remarkably, the model equations require the setting of the latencies τ of the actions of the driver and confounding factor on the target signal regardless of the setting of the driver and the target. In Granger causality analysis, several strategies are present in literature. These strategies can be roughly classified into double-regression and single-regression approaches (74–79). Double-regression approaches lead to a separate identification in the full and restricted universes of knowledge with optimization of the model order in both the universes or in the full universe of knowledge followed by its preservation of the restricted universe. Single-regression approaches are grounded on the optimization of the model order in the full universe of knowledge, and the model parameters in the restricted universe of knowledge are derived from the full structure, where the model order of the reduced structure is modified to be as high as necessary to describe the full decay of the autocovariance. We preferred a double regression approach that requires a separate estimation of the coefficients in the full and restricted universes of knowledge with preservation of the model order (49). However, a fierce debate can be found in literature supporting different strategies because it has been shown that these strategies might lead to different variability in the Granger causality markers (77–79).

DATA AVAILABILITY

Data will be made available upon reasonable request.

GRANTS

This study was partially supported by the Italian Ministry of Health via Ricerca Corrente program to IRCCS Policlinico San Donato and by the Italian Ministry of University and Research (MUR) via the Progetto di Rilevante Interesse Nazionale (PRIN) 2022SLB5MX (to A.P.) (CUP code: G53D23000410006; UGOV code. PRIN202223APORT_01). J.S.M. is supported by a Stroke Association Clinical Lectureship (SA SCLM23\100003) and a UKRI Future Leaders Fellowship (MR/Y016807/1). J.S.M. is supported by the National Institute for Health and Care Research (NIHR) Leicester Biomedical Research Center (BRC). O.L. is supported by a Stroke Association Postdoctoral Fellowship (21\100029).

DISCLAIMERS

The views expressed are those of the authors and not necessarily those of the Stroke Association, UKRI, NIHR, the Department of Health and Social Care, or their employers. The funders had no role in study design, data collection and analysis, decision to publish, or preparation of the manuscript.

DISCLOSURES

No conflicts of interest, financial or otherwise, are declared by the authors.

AUTHOR CONTRIBUTIONS

F.G., B.C., R.B.P., and A.P. conceived and designed research; A.S.M.S., M.Y.L., O.L., and J.S.M. performed experiments; F.G., B.C., V.B., J.I., and A.P. analyzed data; F.G., B.C., B.D.M., O.L., J.I., J.S.M., R.B.P., and A.P. interpreted results of experiments; F.G., B.C., V.B., and A.P. prepared figures; F.G., B.C., and A.P. drafted manuscript; F.G., B.C., V.B., B.D.M., O.L., J.I., J.S.M., R.B.P., and A.P. edited and revised manuscript; F.G., B.C., V.B., B.D.M., A.S.M.S., M.Y.L., O.L., J.I., J.S.M., R.B.P., and A.P. approved final version of manuscript.

REFERENCES

1. **Lassen NA.** Cerebral blood flow and oxygen consumption in man. *Physiol Rev* 39: 183–238, 1959. doi:10.1152/physrev.1959.39.2.183.
2. **Paulson OB**, **Strandgaard S**, **Edvinsson L.** Cerebral autoregulation. *Cerebrovasc Brain Metab Rev* 2: 161–192, 1990.
3. **Aaslid R**, **Lindegaard KF**, **Sorteberg W**, **Nornes H.** Cerebral autoregulation dynamics in humans. *Stroke* 20: 45–52, 1989. doi:10.1161/01.str.20.1.45.
4. **Joshi B**, **Brady K**, **Lee J**, **Easley B**, **Panigrahi R**, **Smielewski P**, **Czosnyka M**, **Hogue CW Jr.** Impaired autoregulation of cerebral blood flow during rewarming from hypothermic cardiopulmonary bypass and its potential association with stroke. *Anesth Analg* 110: 321–328, 2010. doi:10.1213/ANE.0b013e3181c6fd12.
5. **Reinhard M**, **Gerds TA**, **Grabiak D**, **Zimmermann PR**, **Roth M**, **Guschlbauer B**, **Timmer J**, **Czosnyka M**, **Weiller C**, **Hetzel A.** Cerebral dysautoregulation and the risk of ischemic events in occlusive carotid artery disease. *J Neurol* 255: 1182–1189, 2008. doi:10.1007/s00415-008-0865-z.
6. **Castro P**, **Azevedo E**, **Serrador J**, **Rocha I**, **Sorond F.** Hemorrhagic transformation and cerebral edema in acute ischemic stroke: link to cerebral autoregulation. *J Neurol Sci* 372: 256–261, 2017. doi:10.1016/j.jns.2016.11.065.
7. **Carey BJ**, **Manktelow BN**, **Panerai RB**, **Potter JF.** Cerebral autoregulatory responses to head-up tilt in normal subjects and patients with recurrent vasovagal syncope. *Circulation* 104: 898–902, 2001. doi:10.1161/hc3301.094908.
8. **Tarumi T**, **Dunsky DI**, **Khan MA**, **Liu J**, **Hill C**, **Armstrong K**, **Martin-Cook K**, **Cullum CM**, **Zhang R.** Dynamic cerebral autoregulation and tissue oxygenation in amnestic mild cognitive impairment. *J Alzheimers Dis* 41: 765–778, 2014. doi:10.3233/JAD-132018.
9. **Pu L**, **Wang L**, **Zhang R**, **Zhao T**, **Jiang Y**, **Han L.** Projected global trends in ischemic stroke incidence, deaths and disability-adjusted life years from 2020 to 2030. *Stroke* 54: 1330–1339, 2023 [Erratum in *Stroke* 55: e23, 2024]. doi:10.1161/STROKEAHA.122.040073.
10. **Adams HP Jr**, **Bendixen BH**, **Kappelle LJ**, **Biller J**, **Love BB**, **Gordon DL**, **Marsh EE III.** Classification of subtype of acute ischemic stroke. Definitions for use in a multicenter clinical trial. TOAST. Trial of Org 10172 in acute stroke treatment. *Stroke* 24: 35–41, 1993. doi:10.1161/01.str.24.1.35.
11. **Aries MJH**, **Elting JW**, **De Keyser J**, **Kremer BPH**, **Vroomen PCAJ.** Cerebral autoregulation in stroke: a review of transcranial Doppler studies. *Stroke* 41: 2697–2704, 2010. doi:10.1161/STROKEAHA.110.594168.
12. **Castro P**, **Azevedo E**, **Sorond F.** Cerebral autoregulation in stroke. *Curr Atheroscler Rep* 20: 37, 2018. doi:10.1007/s11883-018-0739-5.
13. **Dawson SL**, **Panerai RB**, **Potter JF.** Serial changes in static and dynamic cerebral autoregulation after acute ischaemic stroke. *Cerebrovasc Dis* 16: 69–75, 2003. doi:10.1159/000070118.
14. **Atkins ER**, **Brodie FG**, **Rafelt SE**, **Panerai RB**, **Robinson TG.** Dynamic cerebral autoregulation is compromised acutely following mild ischaemic stroke but not transient ischaemic attack. *Cerebrovasc Dis* 29: 228–235, 2010. doi:10.1159/000267845.
15. **Immink RV**, **van Montfrans GA**, **Stam J**, **Karemaker JM**, **Diamant M**, **van Lieshout JJ.** Dynamic cerebral autoregulation in acute lacunar and middle cerebral artery territory ischemic stroke. *Stroke* 36: 2595–2600, 2005. doi:10.1161/01.STR.0000189624.06836.03.
16. **Petersen NH**, **Ortega-Gutierrez S**, **Reccius A**, **Masurkar A**, **Huang A**, **Marshall RS.** Dynamic cerebral autoregulation is transiently

impaired for one week after large-vessel acute ischemic stroke. *Cerebrovasc Dis* 39: 144–150, 2015. doi:10.1159/000368595.
17. **Tiecks FP**, **Lam AM**, **Aaslid R**, **Newell DW.** Comparison of static and dynamic cerebral autoregulation measurements. *Stroke* 26: 1014–1019, 1995. doi:10.1161/01.str.26.6.1014.
18. **Tiecks FP**, **Lam AM**, **Matta BF**, **Strebel S**, **Douville C**, **Newell DW.** Effects of the Valsalva maneuver on cerebral circulation in healthy adults. A transcranial Doppler study. *Stroke* 26: 1386–1392, 1995. doi:10.1161/01.str.26.8.1386.
19. **Aaslid R**, **Markwalder TM**, **Nornes H.** Noninvasive transcranial Doppler ultrasound recording of flow velocity in basal cerebral arteries. *J Neurosurg* 57: 769–774, 1982. doi:10.3171/jns.1982.57.6.0769.
20. **Panerai RB**, **Dawson SL**, **Potter JF.** Linear and nonlinear analysis of human dynamic cerebral autoregulation. *Am J Physiol Heart Circ Physiol* 277: H1089–H1099, 1999. doi:10.1152/ajpheart.1999.277.3.H1089.
21. **Zhang R**, **Zuckerman JH**, **Giller CA**, **Levine BD.** Transfer function analysis of dynamic cerebral autoregulation in humans. *Am J Physiol Heart Circ Physiol* 274: H233–H241, 1998. doi:10.1152/ajpheart.1998.274.1.h233.
22. **Waltz X**, **Beaudin AE**, **Hanly PJ**, **Mitsis GD**, **Poulin MJ.** Effects of continuous positive airway pressure and isocapnic-hypoxia on cerebral autoregulation in patients with obstructive sleep apnea. *J Physiol* 594: 7089–7104, 2016. doi:10.1113/JP272967.
23. **Diehl RR**, **Linden D**, **Lücke D**, **Berlit P.** Phase relationship between cerebral blood flow velocity and blood pressure. A clinical test of autoregulation. *Stroke*. 26: 1801–1804, 1995. doi:10.1161/01.str.26.10.1801.
24. **Giller CA.** The frequency-dependent behavior of cerebral autoregulation. *Neurosurgery* 27: 362–368, 1990. doi:10.1097/00006123-199009000-00004.
25. **Faes L**, **Porta A**, **Rossato G**, **Adami A**, **Tonon D**, **Corica A**, **Nollo G.** Investigating the mechanisms of cardiovascular and cerebrovascular regulation in orthostatic syncope through an information decomposition strategy. *Auton Neurosci* 178: 76–82, 2013. doi:10.1016/j.autneu.2013.02.013.
26. **Bari V**, **De Maria B**, **Mazzucco CE**, **Rossato G**, **Tonon D**, **Nollo G**, **Faes L**, **Porta A.** Cerebrovascular and cardiovascular variability interactions investigated through conditional joint transfer entropy in subjects prone to postural syncope. *Physiol Meas* 38: 976–991, 2017. doi:10.1088/1361-6579/aa638c.
27. **Porta A**, **Gelpi F**, **Bari V**, **Cairo B**, **De Maria B**, **Tonon D**, **Rossato G**, **Faes L.** Concomitant evaluation of cardiovascular and cerebrovascular controls via Geweke spectral causality to assess the propensity to postural syncope. *Med Biol Eng Comput* 61: 3141–3157, 2023. doi:10.1007/s11517-023-02885-0.
28. **Porta A**, **Gelpi F**, **Bari V**, **Cairo B**, **De Maria B**, **Tonon D**, **Rossato G**, **Ranucci M**, **Faes L.** Categorizing the role of respiration in cardiovascular and cerebrovascular variability interactions. *IEEE Trans Biomed Eng* 69: 2065–2076, 2022. doi:10.1109/TBME.2021.3135313.
29. **Saleem S**, **Teal PD**, **Howe CA**, **Tymko MM**, **Ainslie PN**, **Tzeng Y-C.** Is the Cushing mechanism a dynamic blood pressure-stabilizing system? Insights from Granger causality analysis of spontaneous blood pressure and cerebral blood flow. *Am J Physiol Regul Integr Comp Physiol* 315: R484–R495, 2018. doi:10.1152/ajpregu.00032.2018.
30. **Willie CK**, **Tzeng YC**, **Fisher JA**, **Ainslie PN.** Integrative regulation of human brain blood flow. *J Physiol* 592: 841–859, 2014. doi:10.1113/jphysiol.2013.268953.
31. **Cushing H.** Some experimental and clinical observations concerning states of increased intracranial tension. The Mütter lecture for 1901.*Am J Med Sci* 124: 375–400, 1902.
32. **Dickinson CJ.** Reappraisal of the Cushing reflex: the most powerful neural blood pressure stabilizing system. *Clin Sci (Lond)* 79: 543–550, 1990. doi:10.1042/cs0790543.
33. **Wan WH**, **Ang BT**, **Wang E.** The Cushing response: a case for a review of its role as a physiological reflex. *J Clin Neurosci* 15: 223–228, 2008. doi:10.1016/j.jocn.2007.05.025.
34. **Paton JFR**, **Dickinson CJ**, **Mitchell G.** Harvey Cushing and the regulation of blood pressure in giraffe, rat and man: introducing 'Cushing's mechanism.' *Exp Physiol* 94: 11–17, 2009. doi:10.1113/expphysiol.2008.043455.
35. **McBryde FD**, **Malpas SC**, **Paton JFR.** Intracranial mechanisms for preserving brain blood flow in health and disease. *Acta Physiol (Oxf)* 219: 274–287, 2017. doi:10.1111/apha.12706.
36. **Gelpi F**, **Bari V**, **Cairo B**, **De Maria B**, **Wells R**, **Baumert M**, **Porta A.** Evaluation of cardiovascular and cerebrovascular control mechanisms in postural orthostatic tachycardia syndrome via conditional transfer entropy: the impact of the respiratory signal type. *Physiol Meas* 44: 064001, 2023. doi:10.1088/1361-6579/acdb47.
37. **Yildiz S**, **Thyagaraj S**, **Jin N**, **Zhong X**, **Heidari Pahlavian S**, **Martin BA**, **Loth F**, **Oshinski J**, **Sabra KG.** Quantifying the influence of respiration and cardiac pulsations on cerebrospinal fluid dynamics using real-time phase-contrast MRI. *J Magn Reson Imaging* 46: 431–439, 2017. doi:10.1002/jmri.25591.
38. **Claassen JAHR**, **Meel-van den Abeelen ASS**, **Simpson DM**, **Panerai RB**; **international Cerebral Autoregulation Research Network (CARNet).** Transfer function analysis of dynamic cerebral autoregulation: a white paper from the International Cerebral Autoregulation Research Network. *J Cereb Blood Flow Metab* 36: 665–680, 2016. doi:10.1177/0271678X15626425.
39. **Patel N**, **Panerai RB**, **Haunton V**, **Katsogridakis E**, **Saeed NP**, **Salinet A**, **Brodie F**, **Syed N**, **D'Sa S**, **Robinson TG.** The Leicester Cerebral Haemodynamics Database: normative values and the influence of age and sex. *Physiol Meas* 37: 1485–1498, 2016. doi:10.1088/0967-3334/37/9/1485.
40. **Katsogridakis E**, **Bush G**, **Fan L**, **Birch AA**, **Simpson DM**, **Allen R**, **Potter JF**, **Panerai RB.** Detection of impaired cerebral autoregulation improves by increasing arterial blood pressure variability. *J Cereb Blood Flow Metab* 33: 519–523, 2013. doi:10.1038/jcbfm.2012.191.
41. **Kay SM**, **Marple SL.** Spectrum analysis—a modern perspective. *Proc IEEE* 69: 1380–1419, 1981. doi:10.1109/PROC.1981.12184.
42. **Akaike H.** A new look at the statistical model identification. *IEEE Trans Automat Contr* 19: 716–723, 1974. doi:10.1109/TAC.1974.1100705.
43. **Baselli G**, **Porta A**, **Rimoldi O**, **Pagani M**, **Cerutti S.** Spectral decomposition in multichannel recordings based on multivariate parametric identification. *IEEE Trans Biomed Eng* 44: 1092–1101, 1997. doi:10.1109/10.641336.
44. **Panerai RB**, **Brassard P**, **Burma JS**, **Castro P**, **Claassen JAHR**, **van Lieshout JJ**, **Liu J**, **Lucas SJE**, **Minhas JS**, **Mitsis GD**, **Nogueira RC**, **Ogoh S**, **Payne SJ**, **Rickards CA**, **Robertson AD**, **Rodrigues GD**, **Smirl JD**, **Simpson DM**; **Cerebrovascular Research Network (CARNet).** Transfer function analysis of dynamic cerebral autoregulation: a CARNet white paper 2022 update. *J Cereb Blood Flow Metab* 43: 3–25, 2023. doi:10.1177/0271678X221119760.
45. **Porta A**, **Baselli G**, **Cerutti S.** Implicit and explicit model-based signal processing for the analysis of short term cardiovascular interactions. *Proc IEEE* 94: 805–818, 2006. doi:10.1109/jproc.2006.871774.
46. **Panerai RB**, **White RP**, **Markus HS**, **Evans DH.** Grading of cerebral dynamic autoregulation from spontaneous fluctuations in arterial blood pressure. *Stroke* 29: 2341–2346, 1998. doi:10.1161/01.str.29.11.2341.
47. **Gelpi F**, **Bari V**, **Cairo B**, **De Maria B**, **Tonon D**, **Rossato G**, **Faes L**, **Porta A.** Dynamic cerebrovascular autoregulation in patients prone to postural syncope: comparison of techniques assessing the autoregulation index from spontaneous variability series. *Auton Neurosci* 237: 102920, 2022. doi:10.1016/j.autneu.2021.102920.
48. **Barnett L**, **Barrett AB**, **Seth AK.** Granger causality and transfer entropy are equivalent for Gaussian variables. *Phys Rev Lett* 103: 238701, 2009. doi:10.1103/PhysRevLett.103.238701.
49. **Porta A**, **Faes L**, **Nollo G**, **Bari V**, **Marchi A**, **De Maria B**, **Takahashi ACM**, **Catai AM.** Conditional self-entropy and conditional joint transfer entropy in heart period variability during graded postural challenge. *PLoS One* 10: e0132851, 2015. doi:10.1371/journal.pone.0132851.
50. **Granger CWJ.** Testing for causality: a personal viewpoint. *J Econ Dyn Control* 2: 329–352, 1980. doi:10.1016/0165-1889(80)90069-X.
51. **Porta A**, **Baselli G**, **Rimoldi O**, **Malliani A**, **Pagani M.** Assessing baroreflex gain from spontaneous variability in conscious dogs: role of causality and respiration. *Am J Physiol Heart Circ Physiol* 279: H2558–H2567, 2000. doi:10.1152/ajpheart.2000.279.5.H2558.
52. **Porta A**, **Catai AM**, **Takahashi AC**, **Magagnin V**, **Bassani T**, **Tobaldini E**, **Montano N.** Information transfer through the spontaneous baroreflex in healthy humans. *Methods Inf Med* 49: 506–510, 2010. doi:10.3414/ME09-02-0036.
53. **Porta A**, **Gelpi F**, **Bari V**, **Cairo B**, **De Maria B**, **Panzetti CM**, **Cornara N**, **Bertoldo EG**, **Fiolo V**, **Callus E**, **De Vincentiis C**, **Volpe M**, **Molfetta R**, **Pistuddi V**, **Ranucci M.** Monitoring the evolution of asynchrony between mean arterial pressure and mean cerebral blood

flow via cross-entropy methods. *Entropy (Basel)* 24: 80, 2022. doi:10.3390/e24010080.
54. **Porta A**, **Faes L.** Wiener-Granger causality in network physiology with applications to cardiovascular control and neuroscience. *Proc IEEE* 104: 282–309, 2016. doi:10.1109/JPROC.2015.2476824.
55. **Andrzejak RG**, **Kraskov A**, **Stögbauer H**, **Mormann F**, **Kreuz T.** Bivariate surrogate techniques: necessity, strengths, and caveats. *Phys Rev E Stat Nonlin Soft Matter Phys* 68: 066202, 2003. doi:10.1103/PhysRevE.68.066202.
56. **Bari V**, **Fantinato A**, **Vaini E**, **Gelpi F**, **Cairo B**, **De Maria B**, **Pistuddi V**, **Ranucci M**, **Porta A.** Impact of propofol general anesthesia on cardiovascular and cerebrovascular closed loop variability interactions. *Biomed Signal Process Control* 68: 102735, 2021. doi:10.1016/j.bspc.2021.102735.
57. **Vaini E**, **Bari V**, **Fantinato A**, **Pistuddi V**, **Cairo B**, **De Maria B**, **Ranucci M**, **Porta A.** Causality analysis reveals the link between cerebrovascular control and acute kidney dysfunction after coronary artery bypass grafting. *Physiol Meas* 40: 064006, 2019. doi:10.1088/1361-6579/ab21b1.
58. **Rodbard S**, **Stone W.** Pressor mechanisms induced by intracranial compression. *Circulation* 12: 883–890, 1955. doi:10.1161/01.cir.12.5.883.
59. **Tzeng YC**, **MacRae BA**, **Ainslie PN**, **Chan GS.** Fundamental relationships between blood pressure and cerebral blood flow in humans. *J Appl Physiol (1985)* 117: 1037–1048, 2014. doi:10.1152/japplphysiol.00366.2014.
60. **Tzeng YC**, **Ainslie PN.** Blood pressure regulation IX: cerebral autoregulation under blood pressure challenges. *Eur J Appl Physiol* 114: 545–559, 2014. doi:10.1007/s00421-013-2667-y.
61. **Toska K**, **Eriksen M.** Respiration-synchronous fluctuations in stroke volume, heart rate and arterial pressure in humans. *J Physiol* 472: 501–512, 1993. doi:10.1113/jphysiol.1993.sp019958.
62. **Elstad M**, **O'Callaghan EL**, **Smith AJ**, **Ben-Tal A**, **Ramchandra R.** Cardiorespiratory interactions in humans and animals: rhythms for life. *Am J Physiol Heart Circ Physiol* 315: H6–H17, 2018. doi:10.1152/ajpheart.00701.2017.
63. **Osborn JW.** Hypothesis: set-points and long-term control of arterial pressure. A theoretical argument for a longterm arterial pressure control system in the brain rather than the kidney. *Clin Exp Pharmacol Physiol* 32: 384–393, 2005. doi:10.1111/j.1440-1681.2005.04200.x.
64. **Fan J-L**, **Brassard P**, **Rickards CA**, **Nogueira RC**, **Nasr N**, **McBryde FD**, **Fisher JP**, **Tzeng Y-C.** Integrative cerebral blood flow regulation in ischemic stroke. *J Cereb Blood Flow Metab* 42: 387–403, 2022. doi:10.1177/0271678X211032029.
65. **Marchi A**, **Bari V**, **De Maria B**, **Esler M**, **Lambert E**, **Baumert M**, **Porta A.** Calibrated variability of muscle sympathetic nerve activity during graded head-up tilt in humans and its link with noradrenaline data and cardiovascular rhythms. *Am J Physiol Regul Integr Comp Physiol* 310: R1134–R1143, 2016. doi:10.1152/ajpregu.00541.2015.
66. **Myers MG**, **Norris JW**, **Hachniski VC**, **Sole MJ.** Plasma norepinephrine in stroke. *Stroke* 12: 200–204, 1981. doi:10.1161/01.str.12.2.200.
67. **Salinet ASM**, **Robinson TG**, **Panerai RB.** Effects of cerebral ischemia on human neurovascular coupling, CO_2 reactivity, and dynamic cerebral autoregulation. *J Appl Physiol (1985)* 118: 170–177, 2015. doi:10.1152/japplphysiol.00620.2014.
68. **Ogoh S.** Interaction between the respiratory system and cerebral blood flow regulation. *J Appl Physiol (1985)* 127: 1197–1205, 2019. doi:10.1152/japplphysiol.00057.2019.
69. **Giller CA**, **Bowman G**, **Dyer H**, **Mootz L**, **Krippner W.** Cerebral arterial diameters during changes in blood pressure and carbon dioxide during craniotomy. *Neurosurgery* 32: 737–742, 1993. doi:10.1097/00006123-199305000-00006.
70. **Zhang R**, **Zuckerman JH**, **Iwasaki K**, **Wilson TE**, **Crandall CG**, **Levine BD.** Autonomic neural control of dynamic cerebral autoregulation in humans. *Circulation* 106: 1814–1820, 2002. doi:10.1161/01.CIR.0000031798.07790.FE.
71. **Hamner JW**, **Tan CO**, **Lee K**, **Cohen MA**, **Taylor JA.** Sympathetic control of the cerebral vasculature in humans. *Stroke* 41: 102–109, 2010. doi:10.1161/STROKEAHA.109.557132.
72. **Pernice R**, **Sparacino L**, **Bari V**, **Gelpi F**, **Cairo B**, **Mijatovic G**, **Antonacci Y**, **Tonon D**, **Rossato G**, **Javorka M**, **Porta A**, **Faes L.** Spectral decomposition of cerebrovascular and cardiovascular interactions in patients prone to postural syncope and healthy controls. *Auton Neurosci* 242: 103021, 2022. doi:10.1016/j.autneu.2022.103021.
73. **Sparacino L**, **Antonacci Y**, **Mijatovic G**, **Faes L.** Measuring hierarchically-organized interactions in dynamic networks through spectral entropy rates: theory, estimation, and illustrative application to physiological networks. *Neurocomputing* 630: 129675, 2025. doi:10.1016/j.neucom.2025.129675.
74. **Barnett L**, **Seth AK.** The MVGC multivariate Granger causality toolbox: a new approach to Granger causality inference. *J Neurosci Methods* 223: 50–68, 2014. doi:10.1016/j.jneumeth.2013.10.018.
75. **Dhamala M**, **Liang H**, **Bressler SL**, **Ding M.** Granger-Geweke causality: estimation and interpretation. *NeuroImage* 175: 460–463, 2018. doi:10.1016/j.neuroimage.2018.04.043.
76. **Faes L**, **Stramaglia S**, **Marinazzo D.** On the interpretability and computational reliability of frequency-domain Granger causality. *F1000Res* 6: 1710, 2017. doi:10.12688/f1000research.12694.1.
77. **Stokes PA**, **Purdon PL.** A study of problems encountered in Granger causality analysis from a neuroscience perspective. *Proc Natl Acad Sci USA* 114: E7063–E7072, 2017 [Erratum in *Proc Natl Acad Sci USA* 115: E6964, 2018]. doi:10.1073/pnas.1704663114.
78. **Barnett L**, **Barrett AB**, **Seth AK.** Misunderstandings regarding the application of Granger causality in neuroscience. *Proc Natl Acad Sci USA* 115: E6676–E6677, 2018. doi:10.1073/pnas.1714497115.
79. **Porta A**, **Bari V**, **Cairo B**, **Gelpi F**, **De Maria B**, **Takahashi ACM**, **Catai AM.** On the validity of single regression strategy for Granger causality assessment in cardiovascular and cardiorespiratory control studies. *Annu Int Conf IEEE Eng Med Biol Soc* 2023: 1–4, 2023. doi:10.1109/EMBC40787.2023.10341180.